Available online at www.sciencedirect.com
ScienceDirect
Mathematics and Computers in Simulation 203 (2023) 721–740
MATHEMATICS AND COMPUTERS IN SIMULATION
www.elsevier.com/locate/matcom

Original articles

Modeling metastatic tumor evolution, numerical resolution and growth prediction

I.M. Bulai[a,*], M.C. De Bonis[b], C. Laurita[b], V. Sagaria[b]

[a] *Dipartimento di Scienze Chimiche, Fisiche, Matematiche e Naturali, Università di Sassari, Via Vienna 2, 7100 Sassari, Italy*
[b] *Department of Mathematics, Computer Science and Economics, University of Basilicata, Via dell'Ateneo Lucano 10, 85100 Potenza, Italy*

Received 18 March 2022; received in revised form 21 June 2022; accepted 1 July 2022
Available online 15 July 2022

Abstract

In this paper we consider a generalized metastatic tumor growth model that describes the primary tumor growth by means of an Ordinary Differential Equation (ODE) and the evolution of the metastatic density using a transport Partial Differential Equation (PDE). The numerical method is based on the resolution of a linear Volterra integral equation (VIE) of the second kind, which arises from the reformulation of the ODE–PDE model. The convergence of the method is proved and error estimates are given. The computation of the approximate solution leads to solving well conditioned linear systems. Here we focus our attention on two different case studies: lung and breast cancer. We assume five different tumor growth laws for each of them, different metastatic emission rates between primary and secondary tumors, and lastly that the newborn metastases can be formed by clusters of several cells.

Keywords: Metastatic tumor growth; PDEs; Volterra integral equation; Lung tumor; Breast carcinoma

1. Introduction

The need for better knowledge of the complex biological system which is at the base of the tumor metastatic process is one of the biggest challenges in cancer research. Little is known about the invasion-metastases cascade process that starting from a primary tumor leads to the spread of tumor cells from the original site to a second one within the same organism [8,16,31,32]. Modeling metastatic tumor growth could help for a better understanding of this process [15]. Particularly this provides fundamental tools in estimating the metastatic state in those cases where the small metastases are invisible to the medical devices. A prior knowledge of a patient's metastatic state could help not only in beginning treatment before it evolves into an advanced state but also for a more targeted drug administration [18]. One typology of generally used models are ODE–PDE (Ordinary Differential Equations-Partial Differential Equations) dynamical models, such as the family of age-structured McKendrick–Von Foerster equations. These are models that describe the dynamics of the colony size distribution of multiple metastatic tumors by, first, modeling the growth of the primary tumor size with an ODE, second, modeling the evolution of the metastatic density using a transport PDE, which is characterized by a zero initial condition and a non-local boundary condition

* Corresponding author.
E-mail addresses: imbulai@uniss.it (I.M. Bulai), mariacarmela.debonis@unibas.it (M.C. De Bonis), concetta.laurita@unibas.it (C. Laurita), valeria.sagaria@unibas.it (V. Sagaria).

https://doi.org/10.1016/j.matcom.2022.07.002

for the tumor size (volume or number of cells). Iwata and coauthors in [20], based on the papers [32,33], assumed that the newborn generated metastases are single cells. Later in [14,15] it has been shown that a metastasis generated by the primary tumor can be formed both by single cells and cluster of several cells. More importantly in [9] using a multicolor lineage tracing they have demonstrated that polyclonal seeding by cell clusters is a frequent mechanism in a common mouse model of breast cancer, accounting for >90% of metastases. See also the recent review [22] for more details on the biological principle of metastases. Here, as a first generalization of the model introduced by Iwata and coauthors in [20], we assume that the newborn generated metastases can be formed by clusters of more than one cell.

The growth rate of the metastases, usually, is assumed to be identical to the growth rate of the primary tumor, and the most used growth law is the Gompertz law, although several studies considered tumor growth laws such as logistic, exponential, power-law, etc. [3]. Hence the growth rate of primary tumor size has a key role in metastatic tumor growth dynamics and it is important to study the evolution of different models of the size-structured metastatic density. Benzekry and coauthors, in [3], used data from two different in vivo systems, for lung and breast cancer, to study, validate and compare seven different ODE systems for primary tumor growth process. Based on their results, as a second generalization of Iwata partial differential equation model, here we consider five different tumor growth laws to describe the tumor metastatic growth: exponential, power-law, Gompertz, generalized logistic and von Bertalanffy–West laws, all of them already validated in [3], both for breast and lung cancer. Although, here, we focus our attention only on the case when the metastatic tumor growth law is the same as the one for the primary tumor, the model and the numerical method are introduced for the more general case where the primary and secondary tumors can be characterized by two different growth laws. As a last generalization, but not of minor importance, we also assume that the metastatic emission rate can be different depending if the metastasis originates from the primary or secondary tumors. In fact this question has already been studied in detail by Bethge et al. in [5], for a human hepatocellular carcinoma with metastases in the liver only, by means of a computer model. Recently in [4] it was shown that metastatic emission rates differ substantially between different organs. Therefore, the question must be addressed separately for each tumor type, within a coherent parameter setting that, to the best of our knowledge, is missing. Anyway, in this paper we analyze how changing the emission rate of the primary or secondary tumor will change the metastatic mass.

In order to solve numerically the introduced generalized version of Iwata's model we first reformulate the original PDE model into a Volterra integral equation, in the same fashion of [18]. The benefits of reformulating the model are mainly related to a considerable acceleration and improved accuracy of the numerical model resolution. There exists a wide bibliography for a large variety of numerical methods developed for the solution of linear and nonlinear Volterra integral equations (see, for instance, [1,6,7] and the references therein), Volterra–Fredholm integral equations (see, for instance, [27,28]) and Volterra integro-differential equations (see, for instance, [29]) on finite intervals. Here we are interested in the case of VIEs on infinite intervals, which, to the best of our knowledge, has not been so extensively treated in literature from a numerical point of view.

We use an improved version of the method that was recently proposed in [11] for the numerical computation of long-time solutions of linear VIEs of the second kind, which has the advantage of not being bound to a convolution type VIE as required by the methods based on Fast Fourier Transform techniques (see [17]). It consists, first, in transforming the original VIE into an equivalent one on the positive real semi axis and, after, in solving the latter by means of a Nyström type method. The Nyström discretization is obtained using a truncated product quadrature rule based on Laguerre nodes along with an additional point. A fully discretized version of the method is implemented when the so-called modified moments of the kernel cannot be computed analytically or their computation requires too much effort. In the present paper such modified moments are approximated by means of a truncated quadrature formula based on a set of knots larger than in [11]. Indeed, in the more general case considered here, if, for their computation, we proceed exactly as in [11] the obtained approximating solution is much less accurate (see Tables 3 and 4). Moreover, since the right-hand sides of the VIEs which we have to solve are integrals (see (4)), the numerical method here proposed includes also a suitable approximation of them.

The computation of the approximate solution leads to solving a well conditioned linear system (see Table 5) whose dimension is reduced due to the use of a truncated approximation process. We point out that one needs to solve only one linear system whatever is the number of the evaluation times.

We prove that the improved method is convergent in weighted spaces of continuous functions and error estimates in weighted uniform norm are provided. We remark that such estimates take into account all modifications introduced here and have been proved under sufficient conditions in L^1 norm, which are different from the ones given in [11].

We recall that in [11] the proposed numerical procedure has been tested on some specific linear VIEs of the second kind arising from the reformulation of Iwata PDE model (see [20]) in the case when both the primary and the secondary tumors grow according to the Gompertz growth law and emit metastases with the same emission rate. As observed in [11, p. 484] it allows higher precision than the method used in [18]. However, numerical simulations have shown that if applied to the more general case studies considered here it does not provide results as satisfactory as the ones produced by the method described in this paper.

Some of the questions which we want to answer here by the numerical results are: (i) Using data for two different case studies, lung and breast tumor and studying the model for five different growth laws, are the metastatic mass and the cumulative number of metastases comparable? First, in the same case study but with different growth law, secondly between two different case studies but with the same growth law. (ii) Assuming that the metastatic colonization rate is different depending if the metastasis is generated by the primary tumor or by the metastases themselves, how will this affect the metastatic mass? (iii) Assuming that the metastasis can be released also in clusters of several cells, how will it affect the metastatic mass?

The paper is organized as follows. First we introduce the mathematical modeling framework describing both the general version of Iwata's model and five different tumor growth laws. In Section 2 we present the numerical method used to solve the Volterra integral equation reformulating the starting model with a detailed description of the improvements made with respect to [11]. In Section 3, the proofs of the main results from Section 2 are given. In Section 4 we present the numerical results developed to answer the questions raised above and we end the paper with Section 5 discussing the overall findings and conclusions.

2. The mathematical modeling framework

We consider the following mathematical model to describe the tumor growth and the metastatic spreading

$$\begin{cases} \dfrac{\partial}{\partial t}\rho(v,t) + \dfrac{\partial}{\partial v}[g_m(v)\rho(v,t)] = 0, & v \in [v_{m,0}, b),\ t \geq 0, \\ g_m(v_{m,0})\rho(v_{m,0},t) = \beta_p(v_p(t)) + \displaystyle\int_{v_{m,0}}^{b} \beta_m(v)\rho(v,t)\,dv, & t \in (0,+\infty), \\ \rho(v,0) = 0, & v \in [v_{m,0}, b), \end{cases} \tag{1}$$

where v represents the volume of the tumor, $b > v_{m,0}$ is the volume of the tumor at the saturated level and $v_p(t)$ represents the volume of the primary tumor at time t. The primary tumor is assumed to grow with rate $g_p(v)$ per unit time, i.e. it is the solution of the following Cauchy problem

$$\begin{cases} \dfrac{dv_p(t)}{dt} = g_p(v_p(t)), \quad t \geq 0 \\ v_p(0) = v_{p,0}, \end{cases}$$

where $v_{p,0}$ denotes the volume of the primary tumor at time $t = 0$. The primary tumor is assumed to emit metastases with the rate $\beta_p(v)$ depending on its size. It is further assumed that no metastases are present at time $t = 0$ and that each metastasis becomes a new tumor growing with the rate $g_m(v)$. Then, the volume $v_m(t)$ of a metastasis emitted at time $t = 0$ is the solution of the following Cauchy problem

$$\begin{cases} \dfrac{dv_m(t)}{dt} = g_m(v_m(t)), \quad t \geq 0 \\ v_m(0) = v_{m,0}, \end{cases}$$

where $v_{m,0}$ denotes the volume of the newly created metastases. Finally, each metastasis is assumed to emit new metastases at rate $\beta_m(v)$.

The unknown solution of the model (1) is $\rho(v,t)$ and represents the *metastatic density*, i.e. the colony size distribution with volume v at time t. In many cases the quantity of interest is a biological observable as, for example, the metastatic mass and the cumulative number of metastases (that is the number of metastases greater than a certain volume $\bar{v}$), which can be represented as a weighted integral of the metastatic density $\rho(v,t)$

$$F(t) = \int_{v_{m,0}}^{b} \phi(v)\rho(v,t)\,dv. \tag{2}$$

In particular, denoting by $M(t)$ the total metastatic burden at time t and by $N_{\bar{v}}(t)$ the cumulative number of metastases whose volume is larger than $\bar{v}$, we have

$$F(t) = \begin{cases} M(t) & \text{if } \phi(v) = v \\ N_{\bar{v}}(t) & \text{if } \phi(v) = \chi_{v \geq \bar{v}}(v), \end{cases} \tag{3}$$

where $\chi_{v \geq \bar{v}}$ is the characteristic function of the interval $[\bar{v}, +\infty)$.

Following the results in [18], the PDE model (1) can be reformulated into a Volterra integral equation whose unknown is the biological observable $F(t)$ given by (2)

$$F(t) = \int_0^t \phi(v_m(t-s))\beta_p(v_p(s))\,ds + \int_0^t \beta_m(v_m(t-s))F(s)\,ds.$$

Using a suitable numerical method, one can numerically compute the biological observable $F(t)$ by solving the following VIE

$$F(t) - \int_0^t k(s,t)F(s)\,ds = \int_0^t h(s,t)\,ds \quad t \geq 0, \tag{4}$$

where

$$k(s,t) = \beta_m(v_m(t-s)) \tag{5}$$

and

$$h(s,t) = \phi(v_m(t-s))\beta_p(v_p(s)).$$

In [18–20] the PDE model (1) has been considered in the particular case where:

- $g_p(x) = g_m(x) = a\ x \log \frac{b}{x}$ is the Gompertz growth law;
- $\beta_p(x) = \beta_m(x) = \mu\ x^{\alpha}$ with μ the colonization coefficient and α the fractal dimension of blood vessels infiltrating the tumor;
- $v_{p,0} = v_{m,0} = 10^{-6}$ mm^3 (corresponding to 1 cell [30]).

The values of the four parameters a, b, μ and α involved into the model described above were estimated in [20] in the clinical scenario of a patient having multiple metastatic tumors in the liver with a hepatocellular carcinoma as a primary tumor. The Gompertz growth law covers a wide range of empirical data. However, alternative growth functions can be also considered.

2.1. Different tumor growth laws

In Table 1 we introduce the list of the growth functions $g(t)$ we have used to describe the growth of a tumor volume in time, with the corresponding solution to the Cauchy problem

$$\begin{cases} \dfrac{dv(t)}{dt} = g(v(t)), \quad t \geq 0, \\ v(0) = v_0. \end{cases} \tag{6}$$

In the exponential model the coefficient a is the constant growth rate. This growth law is referred to as exponential v_0 in [3]. The generalized logistic growth law has a sigmoid shape and K represents the carrying capacity that corresponds to the maximal volume of the tumor. The parameter a represents the growth rate related to proliferation kinetics. In the Gompertz model a is the initial proliferation rate (at $v = 1$ mm^3) and β is the rate of exponential decay of a. Last, notice that from the von Bertalanffy–West generalized model assuming $b = 0$, which is the loss term, the power-law model is obtained, where a is once more the growth rate. The exponent γ indicates that the proliferation tissue is proportional to v^{γ}. In all the considered cases, with the exception of the exponential model, we assume $v_0 = 1$ mm^3. Although for the breast data, the dynamics were best captured by the Gompertz model while for lung data, by the Gompertz and power law models (see [3]), here we have chosen to keep also the remaining models studied in [3] taking into account the limits they can bring. For a better description of the models listed in Table 1 see [3].

Table 1
List of all considered growth laws and the corresponding solutions of (6).

Model name	Growth law equation	Solution
Exponential	$\frac{dv}{dt} = av$	$v(t) = v_0 e^{at}$
Generalized logistic	$\frac{dv}{dt} = av\left[1 - \left(\frac{v}{K}\right)^{\nu}\right]$	$v(t) = \frac{v_0 K}{\left[v_0^{\nu} + (K^{\nu} - v_0^{\nu})e^{-a\nu t}\right]^{\frac{1}{\nu}}}$
Gompertz	$\frac{dv}{dt} = ae^{(-\beta t)}v$	$v(t) = v_0 e^{\frac{a}{\beta}(1-e^{-\beta t})}$
Von Bertalanffy–West	$\frac{dv}{dt} = av^{\gamma} - bv$	$v(t) = \left[\frac{a}{b} + \left(v_0^{(1-\gamma)} - \frac{a}{b}\right)e^{-b(1-\gamma)t}\right]^{\frac{1}{1-\gamma}}$
Power-law	$\frac{dv}{dt} = av^{\gamma}$	$v(t) = \left[v_0^{(1-\gamma)} + (1-\gamma)at\right]^{\frac{1}{1-\gamma}}$

2.2. Different emission rate function

As stated before, the emission rate of the metastasis by the primary and the secondary tumors can assume equal or different values. Here we introduce the generalized colonization rate function

$$\beta(x) = \mu_* \, x^{\alpha},$$

simply modifying the colonization coefficient μ_*. Here $* = p$ or $* = m$, depending if the metastasis is emitted by the primary or metastatic tumor, respectively.

3. Numerical method used to solve the Volterra integral equation

In this section we describe the numerical procedure we propose to solve the Volterra integral equation (4). As announced in the Introduction it is based on the method in [11], but proper modifications (that will be better specified later) are introduced in order to improve its efficiency when applied to the general framework described in Section 2.

As a first step, the variable change $s = te^{-z}$ is applied to the integrals in (4) obtaining

$$\int_0^t k(s,t)F(s)\,ds = t\int_0^{+\infty} k(te^{-z},t)F(te^{-z})e^{-z}\,dz \tag{7}$$

and

$$\int_0^t h(s,t)\,ds = t\int_0^{+\infty} h(te^{-z},t)e^{-z}dz.$$

We point out that the above change of variable makes the Laguerre weight function e^{-z} appear under the integral sign in a natural way and allows to apply a Nyström type method using always the same quadrature rule, based at the Laguerre zeros, whatever is the choice of $t \in \mathbb{R}^+$. Then, letting

$$(KF)(t) = t\int_0^{+\infty} k(te^{-z},t)F(te^{-z})e^{-z}\,dz,$$

$$G(t) = t\int_0^{+\infty} h(te^{-z},t)e^{-z}dz \tag{8}$$

and denoting by I the identity operator, the VIE (4) can be written in the following more compact form

$$(I - K)F = G. \tag{9}$$

As a second step, a Nyström type method is applied to the above equation in order to approximate its solution. The numerical method is based on the approximation of the integral $(KF)(t)$ by a product quadrature rule. More precisely, the unknown F is replaced by a truncated version of the Lagrange polynomial interpolating it at the zeros $z_{n,1}, z_{n,2}, \ldots, z_{n,n}$ of the Laguerre polynomial $p_n(w)$ of degree n and at the additional point $4n$. Here $w(x)$ denotes the Laguerre weight function e^{-x}. We recall that (see, for example, [10,23,26]) such truncated polynomial, denoted

by $L^*_{n+1}(F,t)$, is defined as follows

$$L^*_{n+1}(F,t) = \sum_{i=1}^{j} \ell_{n+1,i}(t) F(z_{n,i}),$$

where

$$j = \min_{i=1,\dots,n} \{i \ : \ z_{n,i} \geq 4\theta n\}, \tag{10}$$

with $0 < \theta < 1$ fixed, and

$$\ell_{n+1,i}(t) = l_{n,i}(t) \frac{4n - t}{4n - z_{n,i}}, \quad i = 1, \dots, j,$$

with $l_{n,i}(t) = \frac{p_n(w,t)}{p'_n(w,z_{n,i})(t-z_{n,i})}$ the ith fundamental Lagrange polynomial associated with the system of interpolation nodes $\{z_{n,i}\}_{i=1,\dots,n}$. We obtain

$$\begin{aligned}(K_n F)(t) &= t \int_0^{+\infty} k(te^{-z}, t) L^*_{n+1}(F, te^{-z}) e^{-z} dz \\ &= \sum_{i=1}^{j} F(z_{n,i}) \ t \int_0^{+\infty} k(te^{-z}, t) \ell_{n+1,i}(te^{-z}) e^{-z} \, dz \\ &=: \sum_{i=1}^{j} F(z_{n,i}) c_i(t). \end{aligned} \tag{11}$$

Since in most cases the analytical expressions of the modified moments $c_i(t)$, $i = 1, \dots, j$, are not available, we approximate them by a quadrature formula. As in [11, p. 480] our choice falls on a truncated Gauss–Laguerre rule [25], but here we propose to apply it with a number N of knots much larger than n in order to increase the accuracy in the computation of the integrals $c_i(t)$. More precisely, they are approximated by the quantities

$$c_{i,N}(t) = t \sum_{\nu=1}^{J} \lambda_\nu k(te^{-z_{N,\nu}}, t) \ell_{n+1,i}(te^{-z_{N,\nu}}), \tag{12}$$

where $z_{N,\nu}$ is the νth zero of the Laguerre polynomial $p_N(w)$, λ_ν is the corresponding Christoffel number and

$$J = \min_{\nu=1,\dots,N} \{\nu \ : \ z_{N,\nu} \geq 4\theta N\}, \tag{13}$$

with $0 < \theta < 1$ fixed. Then, we get the new discrete operator

$$(K_{n,N} F)(t) = \sum_{i=1}^{j} F(z_{n,i}) c_{i,N}(t) = t \sum_{\nu=1}^{J} \lambda_\nu k(te^{-z_{N,\nu}}, t) L^*_{n+1}(F, te^{-z_{N,\nu}})$$

which can be also regarded as the approximation of $(K_n F)(t)$ by means of the N-point truncated Gaussian rule. Finally, we apply the same N-point truncated Gauss–Laguerre quadrature formula for approximating the right-hand side integral $G(t)$ given in (8), obtaining

$$G_N(t) = t \sum_{\nu=1}^{J} \lambda_\nu h(te^{-z_{N,\nu}}, t). \tag{14}$$

Note that in [11, Subsection 4.1] the truncated Gauss–Laguerre rule has been applied to the right-hand side integrals using only n quadrature knots. Nevertheless, since the theoretical error analysis has been carried out for a general VIE, these approximations have not been considered, differently from what we are going to do in this paper (see Theorem 3.3). Therefore, the integral equation (9) is approximated by the following finite-dimensional equation

$$(I - K_{n,N}) F_{n,N} = G_N, \tag{15}$$

in the unknown $F_{n,N}$.

In order to compute the solution $F_{n,N}$ of (15), first both sides of Eq. (15) are multiplied by the weight $u(t) = t^{\gamma}(1+t)^{\delta}e^{-\frac{t}{2}}$, $\gamma, \delta \geq 0$, getting

$$(F_{n,N}u)(t) - u(t)\sum_{i=1}^{j}\frac{(F_{n,N}u)(z_{n,i})}{u(z_{n,i})}c_{i,N}(t) = (G_N u)(t). \tag{16}$$

Then, Eq. (16) is collocated at the Laguerre nodes $z_{n,i}$, $i = 1, \ldots, j$, and the following linear system of order j is obtained

$$\sum_{i=1}^{j}\left[\delta_{r,i} - \frac{u(z_{n,r})}{u(z_{n,i})}c_{i,N}(z_{n,r})\right]a_i = (G_N u)(z_{n,r}), \quad r = 1, \ldots, j, \tag{17}$$

in the unknowns $a_i = (F_{n,N}u)(z_{n,i})$, $i = 1, \ldots, j$. Finally, once the linear system is solved, the Nyström interpolating function

$$F_{n,N}(t) = G_N(t) + \sum_{i=1}^{j}\frac{c_{i,N}(t)}{u(z_{n,i})}a_i \tag{18}$$

is constructed. If $(a_1, \ldots, a_j)$ is a solution of the system (17), then the Nyström interpolating function $F_{n,N}$ is a solution of Eq. (15) and viceversa.

We remark that as time t changes, we have to calculate only the Nyström interpolant (18) without solving a new linear system and for this a crucial role is played by the change of variable adopted in (7).

Now, in order to provide sufficient conditions ensuring the unisolvence of Eq. (9), the convergence of the just described method and the well conditioning of the linear systems (17), we need the following definitions.

Let us consider the set L^1 of all measurable functions $f : \mathbb{R}^+ \to \mathbb{R}$ such that

$$\|f\|_{L^1} = \|f\|_1 = \int_0^{+\infty}|f(s)|ds < +\infty$$

and its Sobolev-type subspace W_r^1, $r \in \mathbb{N}$, defined as follows

$$W_r^1 = \left\{f \in L^1 : \ f^{(r-1)} \in AC(0,+\infty), \ \|f^{(r)}\varphi^r\|_1 < +\infty\right\},$$

with $\varphi(t) = \sqrt{t}$ and $AC(A)$ the collection of all functions which are absolutely continuous on every closed subset $A \subseteq (0,+\infty)$, equipped with the norm

$$\|f\|_{W_r^1} = \|f\|_1 + \|f^{(r)}\varphi^r\|_1.$$

For a fixed $t \in \mathbb{R}^+$, we will also consider the spaces $L_1([0,t])$ and $W_r^1([0,t])$ defined as L^1 and W_r^1, respectively, but with the interval $[0,+\infty)$ replaced by $[0,t]$.

Moreover, we set

$$\rho(f) = \int_0^{+\infty}|f(s)|(1+\log^+|f(s)|)ds,$$

where $\log^+(s) = \log(\max\{1,s\})$, for $s > 0$.

For a weight function

$$u(t) = t^{\gamma}(1+t)^{\delta}e^{-\frac{t}{2}}, \quad \gamma, \delta \geq 0,$$

we indicate with C_u the function space defined as

$$C_u = \left\{f \in C((0,+\infty)) : \lim_{\substack{t\to 0^+\\ t\to+\infty}}(fu)(t) = 0\right\}, \quad \text{if} \quad \gamma > 0,$$

or

$$C_u = \left\{f \in C([0,+\infty)) : \lim_{t\to+\infty}(fu)(t) = 0\right\}, \quad \text{if} \quad \gamma = 0,$$

and endowed with the weighted norm

$$\|f\|_u = \sup_{t\geq 0}|(fu)(t)|.$$

Finally, for a positive integer r, we consider the Sobolev-type subspace of C_u of order r

$$W_{r,u} = \{f \in C_u : f^{(r-1)} \in AC((0,+\infty)),\ \|f^{(r)}\varphi^r\|_u < +\infty\},$$

and we equip $W_{r,u}$ with the following norm

$$\|f\|_{W_{r,u}} = \|f\|_u + \|f^{(r)}\varphi^r\|_u.$$

In particular, we set $W_{0,u} = C_u$. In what follows the notations $k_t(s)$ and $k_s(t)$ will be used to refer to $k(s,t)$ regarded as a function of the only variable s or t, respectively. With an analogous meaning we will also use the notation $h_t(s)$ and $h_s(t)$ for the bivariate function $h(s,t)$.

Theorem 3.1. *Let $u(t) = t^\gamma(1+t)^\delta e^{-\frac{t}{2}}$ with $\gamma \le \frac{1}{4}$ and $\delta \ge \frac{1}{4} - \gamma$. Let us assume that the kernel $k(s,t)$ satisfies*

$$\sup_{t\ge 0} u(t) \left\| \frac{k_t}{u} \right\|_1 < +\infty, \tag{19}$$

$$\sup_{t\ge 0} u(t)\rho\left(\frac{k_t}{\sqrt{w\varphi}}\right) < +\infty, \tag{20}$$

and

$$\lim_{h\to 0} \sup_{t\ge 0} \rho\left(\frac{u(t+h)k_{t+h} - u(t)k_t}{\sqrt{w\varphi}}\right) = 0.$$

If $\mathrm{Ker}(I-K) = \{0\}$ *in C_u, then Eq. (9) is unisolvent for any $h(s,t)$ such that*

$$\lim_{t\to+\infty} u(t) \int_0^t h(s,t)ds = 0 \tag{21}$$

and

$$\sup_{t\ge 0} u(t)\, \|h_t\|_{L^1([0,t])} < +\infty. \tag{22}$$

Theorem 3.2. *Let us assume that the assumptions of Theorem 3.1 are satisfied for $\gamma = \frac{1}{4}$ and $\delta \ge 0$. Further assume that, for any $r \ge 1$,*

$$\sup_{0<t<1} u(t)\varphi(t) \left\| \frac{\varphi^i}{u} k_t^{(i)} \right\|_1 < +\infty, \quad i = 0,\dots,r, \tag{23a}$$

$$\sup_{t\ge 1} u(t)\varphi^r(t) \left\| \frac{\varphi^i}{u} k_t^{(i)} \right\|_1 < +\infty, \quad i = 0,\dots,r. \tag{23b}$$

Then, for all sufficiently large n (say $n \ge n_0$), the coefficient matrix $A_{n,N}$ of system (17) is invertible and its condition number in uniform norm satisfies

$$\sup_{n\ge n_0} \mathrm{cond}(A_{n,N}) \le \mathcal{C}, \qquad \mathcal{C} \ne \mathcal{C}(n). \tag{24}$$

Theorem 3.3. *Let us assume that the assumptions of Theorem 3.2 are satisfied and that, for some $r \ge 1$, the function $h(s,t)$ satisfies (21), (22) and*

$$\sup_{0<t<1} u(t)\varphi(t)\, \|h_t\|_{W_r^1([0,t])} < +\infty, \tag{25a}$$

$$\sup_{t\ge 1} u(t)\varphi^r(t)\, \|h_t\|_{W_r^1([0,t])} < +\infty. \tag{25b}$$

If we further suppose that, for all sufficiently large n (say $n \ge n_0$), the inverse operators $(I - K_{n,N})^{-1} : C_u \to C_u$ exist and are uniformly bounded w.r.t. n and that the exact solution F of (4) belongs to $W_{r,u}$, then the Nyström interpolant $F_{n,N}$ in (18) satisfies the following error estimate

$$\|F - F_{n,N}\|_u \le \mathcal{C} \max\left\{\frac{1}{n^{\frac{r}{2}}}, \frac{\log n}{N^{\frac{r}{2}}}\right\}, \tag{26}$$

where $\mathcal{C} \ne \mathcal{C}(n,N)$.

Assuming the stability of the method, we are able to give the above error estimate showing how the convergence order depends on the smoothness of the solution. Although we are not able to provide the theoretical proof of the stability, we remark that the method can be regarded as a proper combination of the stable method proposed in [11, (21) and Theorem 3.1] (see also the proof of Theorem 3.2) and the stable truncated Gauss–Laguerre quadrature rule (see [25]), used for approximating the modified moments $c_i(t)$, $i = 1, \dots, j$ (see (12)). Anyway, the stability and convergence are both amply demonstrated by numerical evidence. In particular, the values of the condition numbers, which do not increase as the dimension of the linear system grows, confirm that the method is actually stable, (see Table 5 in Section 5).

Moreover, inspecting error estimate (26) one can see that if, as done in [11, Subsection 4.1], we approximate both the modified moments $c_i(t), i = 1, \dots, j$, and the right-hand side $G(t)$ given in (8) by a n-point Gaussian quadrature rule, we get the worst rate of convergence $n^{-\frac{r}{2}} \log n$. Then, the better performances obtained with the use of a truncated Gauss–Laguerre rule based on N knots with $N \gg n$ (see Tables 3 and 4 in Section 5) agree with the theoretical expectations in the weighted space C_u where the solution lives (see Theorem 3.1). However, the unweighted error in uniform norm could become as greater as t is larger, then in the numerical simulations we have introduced a suitable scaling parameter $\mathcal{K}$ that let us avoid this drawback.

We also highlight that in the above theorems we give conditions on the known functions involved in the VIE w.r.t. the L^1 norm which are easier to be verified than ones in infinity norm provided in [11, Theorems 2.3 and 3.2].

4. Proofs

Proof of Theorem 3.1. Using Theorem 2.3 in [11] it is possible to deduce that the equation $(I - K)F = g$ admits a unique solution for any $g \in C_u$. It is easy to see that if the right-hand side $g(t)$ is the function $G(t)$ defined in (8), the assumptions (21) and (22) imply $G \in C_u$. In fact

$$|G(t)|u(t) = u(t)\left|\int_0^t h(s,t)ds\right|. \quad \square$$

In order to prove Theorems 3.2 and 3.3 we need the following lemma.

Lemma 1. *Let $u(t) = t^\gamma(1+t)^\delta e^{-\frac{t}{2}}$ with $\gamma = \frac{1}{4}$, $\delta \geq 0$ and $r \geq 1$. For $F \in W_{r,u}$, if the kernel $k(s,t)$ satisfies (20) and (23), we have*

$$\|K_n F - K_{n,N} F\|_u \leq \frac{\mathcal{C}}{N^{\frac{r}{2}}} \log n \|F\|_{W_{r,u}},$$

where $\mathcal{C} \neq \mathcal{C}(n, N, F, k_t)$.

Proof. Since $(K_{n,N}F)(t)$ is the approximation of $(K_n F)(t)$ by means of the truncated Gaussian rule [25] we have

$$u(t)|(K_n F)(t) - (K_{n,N}F)(t)| = u(t)t|R_N(\bar{H}_t)|, \tag{27}$$

where $R_N(\bar{H}_t)$ is the quadrature error related to the function $\bar{H}_t(z) = H(te^{-z}, t)$ with $H(s,t) = k(s,t)L^*_{n+1}(F,s)$. Using estimate [25, Corollary 2.4], we get

$$u(t)t|R_N(\bar{H}_t)| \leq \mathcal{C}u(t)t\left[\frac{\|\bar{H}_t^{(r)}\varphi^r w\|_1}{N^{\frac{r}{2}}} + e^{-AN}\|\bar{H}_t w\|_1\right]. \tag{28}$$

Taking into account [21, Lemma 9] (see also [11, Lemma 2.2]), under the assumption (20), we have

$$\begin{aligned} u(t)t\|\bar{H}_t w\|_1 &= u(t)\left|\int_0^t k(s,t)L^*_{n+1}(F,s)ds\right| \\ &\leq \int_0^{+\infty} |u(t)k(s,t)||L^*_{n+1}(F,s)|ds \\ &\leq \mathcal{C}\|F\|_u. \end{aligned} \tag{29}$$

Note that

$$|\bar{H}_t^{(r)}(z)\varphi^r(z)w(z)| \leq \mathcal{C}(r)\varphi^r(z)w(z)\sum_{i=1}^{r}\left|H_t^{(i)}(te^{-z})(te^{-z})^{\frac{i}{2}}\right|(te^{-z})^{\frac{i}{2}},$$

where the notation $H_t(s)$ refers to $H(s,t)$ regarded as a function of variable s. Then, by [13, Lemma 2.1],

$$\begin{aligned} u(t)t\|\bar{H}_t^{(r)}\varphi^r w\|_1 &\le \mathcal{C}(r)u(t)\sum_{i=1}^{r}\int_0^{+\infty}\left|H_t^{(i)}(te^{-z})(te^{-z})^{\frac{i}{2}}\right| z^{\frac{r}{2}}(te^{-z})^{\frac{i}{2}}te^{-z}dz \\ &\le \mathcal{C}(r)u(t)\sum_{i=1}^{r}\int_0^{t}\left|H_t^{(i)}(s)s^{\frac{i}{2}}\right|\log^{\frac{r}{2}}\left(\frac{t}{s}\right)s^{\frac{i}{2}}ds \\ &\le \mathcal{C}(r)t^{\frac{\ell}{2}}u(t)\sum_{i=0}^{r}\int_0^{t}\left|H_t^{(i)}(s)s^{\frac{i}{2}}\right|ds \\ &\le \mathcal{C}(r)t^{\frac{\ell}{2}}u(t)\left[\|H_t\|_1+\|H_t^{(r)}\varphi^r\|_1\right], \end{aligned} \tag{30}$$

where $\ell = 1$ for $0 < t < 1$ and $\ell = r$ for $t \ge 1$. By [24] (see also [11, (11)]), under the assumption (23) with $i = 0$, we have

$$\begin{aligned} t^{\frac{\ell}{2}}u(t)\|H_t\|_1 &\le \mathcal{C}\int_0^{+\infty}\frac{t^{\frac{\ell}{2}}u(t)}{u(s)}|k_t(s)||[L_{n+1}^*(F,s)]u(s)|ds \\ &\le \mathcal{C}\log n\|F\|_u\int_0^{+\infty}\frac{t^{\frac{\ell}{2}}u(t)}{u(s)}|k_t(s)|ds \\ &\le \mathcal{C}\log n\|F\|_u. \end{aligned}$$

From [11, (13)] and [12, proof of Lemma 6.3, p. 148], under the assumption (23), we deduce

$$\begin{aligned} t^{\frac{\ell}{2}}u(t)\|H_t^{(r)}\varphi^r\|_1 &\le \mathcal{C}\sum_{i=0}^{r}\int_0^{+\infty}\frac{t^{\frac{\ell}{2}}u(t)}{u(s)}|k_t^{(r-i)}(s)\varphi^{r-i}(s)||[L_{n+1}^*(F,s)]^{(i)}\varphi^i(s)u(s)|ds \\ &\le \mathcal{C}\sum_{i=0}^{r}\|[L_{n+1}^*(F)]^{(i)}\varphi^i\|_u\int_0^{+\infty}\frac{t^{\frac{\ell}{2}}u(t)}{u(s)}|k_t^{(r-i)}(s)\varphi^{r-i}(s)|ds \\ &\le \mathcal{C}\log n\sum_{i=0}^{r}\|F\|_{W_{i,u}}\int_0^{+\infty}\frac{t^{\frac{\ell}{2}}u(t)}{u(s)}|k_t^{(r-i)}(s)\varphi^{r-i}(s)|ds \\ &\le \mathcal{C}\log n\|F\|_{W_{r,u}}. \end{aligned}$$

Consequently

$$u(t)t\|\bar{H}_t^{(r)}\varphi^r w\|_1 \le \mathcal{C}\log n\|F\|_{W_{r,u}}.$$

Combining the last inequality with (29), (27) and (28), the thesis follows. □

Proof of Theorem 3.2. Let us consider the finite dimensional equation

$$(I - K_n)F_n = G, \tag{31}$$

where K_n is the operator defined in (11). Proceeding as done in [11, p. 6], it is easy to deduce the equivalent linear system

$$\sum_{i=1}^{j}\left[\delta_{r,i} - \frac{u(z_{n,r})}{u(z_{n,i})}\,c_i(z_{n,r})\right]a_i = (Gu)(z_{n,r}), \quad r = 1,\dots,j, \tag{32}$$

whose solutions $a_i = (F_n u)(z_{n,i})$, $i = 1,\dots,j$, can be used to construct the unknown function of Eq. (31) as follows

$$F_n(t) = G(t) + \sum_{i=1}^{j}\frac{c_i(t)}{u(z_{n,i})}a_i.$$

By [11, Theorem 3.1], for sufficiently large n (say $n \geq n_0$) the inverse operators $(I - K_n)^{-1} : C_u \to C_u$ exist and are uniformly bounded. Moreover, denoted by A_n the coefficient matrix of system (32), one has

$$\sup_{n \geq n_0} \text{cond}(A_n) \leq \mathcal{C} \neq \mathcal{C}(n). \tag{33}$$

Following the same steps of the proof of [11, Theorem 3.2] but using Lemma 1 in place of [11, Lemma 5.5], it is possible to prove that $(A_{n,N})^{-1}$ exists for sufficiently large n and

$$\lim_n \frac{\text{cond}(A_{n,N})}{\text{cond}(A_n)} = 1.$$

Then, (24) easily follows from (33). □

Proof of Theorem 3.3. In order to prove (26), we first note that

$$(F - F_{n,N}) = (I - K_{n,N})^{-1}[(G - G_N) - (K - K_{n,N})F].$$

Then, under the assumption

$$\sup_{n \geq n_0} \|(I - K_{n,N})^{-1}\|_u \leq \mathcal{C}, \quad \mathcal{C} \neq \mathcal{C}(n),$$

we get, for $n \geq n_0$,

$$\|F - F_{n,N}\|_u \leq \mathcal{C}\left(\|G - G_N\|_u + \|(K - K_{n,N})F\|_u\right). \tag{34}$$

Now, since

$$\|(K - K_{n,N})F\|_u \leq \|(K - K_n)F\|_u + \|(K_n - K_{n,N})F\|_u,$$

if the unknown solution F of (9) belongs to $W_{r,u}$, for some $r \geq 1$, using [11, (41) and (8)] and Lemma 1, we have

$$\|(K - K_{n,N})F\|_u \leq \frac{\mathcal{C}}{n^{\frac{r}{2}}}\|F\|_{W_{r,u}} + \frac{\mathcal{C}}{N^{\frac{r}{2}}}\log n \|F\|_{W_{r,u}}, \quad n \geq n_0, \quad \mathcal{C} \neq \mathcal{C}(n, F). \tag{35}$$

Concerning $\|G - G_N\|_u$, we recall that $G_N(t)$ is the approximation of the integral $G(t)$ by means of the truncated Gauss–Laguerre quadrature rule [25]. Then, we have

$$u(t)|G(t) - G_N(t)| = u(t)t|R_N(\bar{h}_t)|, \tag{36}$$

where $R_N(\bar{h}_t)$ is the quadrature error related to the function $\bar{h}_t(z) = h(te^{-z}, t)$. Using estimate [25, Corollary 2.4], we get

$$u(t)t|R_N(\bar{h}_t)| \leq \mathcal{C}u(t)t\left[\frac{\|\bar{h}_t^{(r)}\varphi^r w\|_1}{N^{\frac{r}{2}}} + e^{-AN}\|\bar{h}_t w\|_1\right].$$

Moreover

$$u(t)t\|\bar{h}_t w\|_1 = u(t)\left|\int_0^t h(s,t)ds\right| = u(t)\|h_t\|_{L^1([0,t])}$$

and, proceeding as in (30) replacing H_t with h_t,

$$u(t)t\|\bar{h}_t^{(r)}\varphi^r w\|_1 \leq \mathcal{C}(r)t^{\frac{\ell}{2}}u(t)\left[\|h_t\|_{L^1([0,t])} + \|h_t^{(r)}\varphi^r\|_{L^1([0,t])}\right], \tag{37}$$

where $\ell = 1$ for $0 < t < 1$ and $\ell = r$ for $t \geq 1$. Then, combining (36)–(37), under the assumptions (21) and (25) we deduce

$$\|G - G_N\|_u \leq \frac{\mathcal{C}}{N^{\frac{r}{2}}}, \quad \mathcal{C} \neq \mathcal{C}(h).$$

Substituting the above inequality and (35) into (34), (26) follows. □

Table 2
Parameter values for five different growth laws (Table 1) computed in [3] for lung and breast data.

Model	Par. Name	Value (Lung)	Value (Breast)	Unit
Exponential	$v_{p,0}$	13.2	68.2	mm^3
	a	0.257	0.0846	day^{-1}
Generalized logistic	a	2555	2753	day^{-1}
	K	4378	1964	mm^3
	ν	$1.4e{-}04$	$2.68e{-}05$	–
Gompertz	a	0.743	0.56	day^{-1}
	β	0.0792	0.0719	day^{-1}
Von Bertalanffy–West	a	7.72	2.32	$mm^{3(1-\gamma)}day^{-1}$
	γ	0.947	0.918	–
	b	6.75	0.808	day^{-1}
Power-law	a	0.921	1.32	$mm^{3(1-\gamma)}day^{-1}$
	γ	0.788	0.58	–

Table 3
Relative errors $e_{256,N}(M,t)$ obtained approximating the metastatic mass in the case of breast data using the following growth laws: generalized logistic (gen log), von Bertalanffy–West (von bert) and power-law (power).

t	gen log		von bert		power	
	$N=256$	$N=2048$	$N=256$	$N=2048$	$N=256$	$N=2048$
10	$1.92e{-}12$	0	$1.49e{-}15$	0	$8.51e{-}09$	$1.06e{-}15$
20	$1.92e{-}12$	0	$1.49e{-}15$	0	$1.76e{-}08$	$1.06e{-}15$
50	$5.46e{-}12$	$2.15e{-}16$	$8.56e{-}11$	$3.34e{-}16$	$3.93e{-}07$	$5.62e{-}14$
100	$8.43e{-}09$	$9.90e{-}15$	$4.86e{-}07$	$5.24e{-}10$	$3.00e{-}06$	$1.54e{-}15$

5. Numerical simulations

For the numerical simulations we have written a MatLab Toolbox called VIE Toolbox which contains fourteen MatLab functions implementing the numerical method described in Section 3. This toolbox is licensed under the GNU General Public License v3.0 and is freely available through https://github.com/IuliaMartinaBulai/VIE_Toolbox. Using VIE Toolbox we will see how the total metastatic mass $M(t)$ and the cumulative number of metastases $N_{\bar{v}}(t)$ (whose volumes are larger than a certain size $\bar{v}$) change assuming five different tumor growth laws (see Table 1 for more details).

We will analyze two different case studies using data introduced in [3] for lung and breast tumors. Moreover, we will show the results obtained for the metastatic mass and the number of metastases in the more general case where the metastatic emission rate is different for the primary tumor and for the metastatic one. Last, we will consider the cases where the emitted metastases have initial sizes greater than 10^{-6} $mm^3 = 1$ cell.

As one can see in Table 2, some of the parameters involved in the definition of the growth laws listed in Table 1 (see [3]) depend on time t expressed in days. Then, the method computes the biological observables as functions of the number of days. If we multiply these parameters by a coefficient $\mathcal{K}$, the method provides approximations of the observables related to $\mathcal{K}t$ days, in correspondence of the input parameter t. Since the computation of the unweighted approximated solutions $F_{n,N}(t)$ can be affected by loss of accuracy when t becomes large (we recall that by Theorem 3.1 the solution of the VIE (4) belongs to the weighted space C_u), a suitable choice of the scaling parameter $\mathcal{K}$ is crucial to improve the performances of the method for large numbers of days.

The numerical method essentially consists in solving the linear system (17) of order j, where j is defined in (10), and in computing the approximate solution $F_{n,N}$ by using (18). Choosing j and J in (10) and (13), respectively, with $\theta = \frac{1}{4}$ and letting

$$e_{n,N}(F,t) = \frac{|F_{512,N}(t) - F_{n,N}(t)|}{|F_{512,N}(t)|},$$

where F is defined in (3), in Tables 3 and 4 we compare the numerical results obtained using the numerical method introduced in [11] ($N = n$ and $j = J$) and its improved version proposed here ($N \gg n$).

Table 4
Relative errors $e_{256,N}(N_{\bar{v}}, t)$ obtained approximating the cumulative number of metastases greater than $\bar{v} = 10^{-6}$ mm^3 in the case of breast data using the following growth laws: generalized logistic (gen log), von Bertalanffy–West (von bert) and power-law (power).

t	gen log		von bert		power	
	$N = 256$	$N = 2048$	$N = 256$	$N = 2048$	$N = 256$	$N = 2048$
10	5.30e−13	0	1.45e−15	0	5.17e−09	0
20	1.49e−12	0	1.45e−15	1.91e−16	3.45e−08	1.81e−16
50	1.57e−12	3.52e−15	8.02e−11	2.23e−14	4.23e−07	4.07e−16
100	1.18e−08	2.06e−14	4.85e−07	4.13e−15	3.25e−06	2.13e−15

It is evident that, as previously announced, the modifications brought here to the method in [11] let us to compute approximations of the observables that are much more accurate. We report only the results obtained in the case of breast data but analogous results can be obtained in the case of lung data.

In all the numerical simulations that follow, the parameters $\mathcal{K}$, n, N, j, and J involved in the implementation of the method have been chosen such that the relative errors

$$e_{n,N}(F) = \max_{t\in\{1,\dots,60\}} e_{n,N}(F,t),$$

are at least of the order of $0.5e-10$. We point out that in many cases the method provides smaller relative errors (for example, in the resolution of the equations obtained using the Gompertz, the exponential and the power laws the relative errors are of the order of the machine precision).

In particular, we have taken $\mathcal{K} = 1$, $n = 256$ and we have computed j by (10) choosing $\theta = \frac{1}{4}$ (so $j = 156$). In order to evaluate $c_{i,N}(t)$, $i = 1, \dots, j$, and $G_N(t)$ we have chosen $N = 2048$ and dynamically detected J according to the following criteria

$$J = J_t^* := \min_{\nu=1,\dots,N}\{\nu : |t\lambda_\nu k(te^{-z_{N,\nu}}, t)L_{n+1}^*(f, te^{-z_{N,\nu}})| < 0.5e-25\} \tag{38}$$

in (12) and

$$J = \bar{J}_t := \min_{\nu=1,\dots,N}\{\nu : |t\lambda_\nu h(te^{-z_{N,\nu}}, t)| < 0.5e-25\} \tag{39}$$

in (14), respectively. We remark that the above definitions of J are equivalent to (13) in the sense that there exists a $\theta \in (0,1)$ s.t. $z_{N,J-1} < 4\theta N < z_{N,J}$, with J defined in (38) or (39).

Concerning the computational complexity of the method, the most computational effort is due to the construction of the entries of the matrix and the right-hand side of the linear system which requires $\mathcal{O}(j^2J^*)$ and $\mathcal{O}(j\bar{J})$ function evaluations, respectively, where $J^* = \max_{r=1,\dots,j} J^*_{z_{n,r}}$ and $\bar{J} = \max_{r=1,\dots,j} \bar{J}_{z_{n,r}}$. Moreover, for any choice of t, further $\mathcal{O}(\bar{J}_t + jJ_t^*)$ function evaluations are needed in the computation of the Nyström interpolant (18). We point out that the use of $N = 2048$ does not lead to a significant increase in the computational cost. In fact, in all the performed numerical tests we have got $J^* \le 278$, $\bar{J} \le 302$, $J_t^* \le 232$ and $\bar{J}_t \le 235$.

Although the sufficient conditions (19)–(23) and (25) are not satisfied by the kernels $k(s,t)$ and $h(s,t)$ for von Bertalanffy–West and power-law growth laws and, hence, the convergence of the method and the well-conditioning of the solved linear systems are not theoretically guaranteed, they are proved by numerical evidence. Looking for less stringent sufficient conditions will be an argument for future investigation.

Finally, we highlight that, according to (24), the matrices of coefficients $A_{n,N}$ of linear systems (17) are always well conditioned. Taking into account that the kernel $k(s,t)$ in (5) depends only on the choice of β_m (and then of μ_m) and g_m, the method leads to solve the same linear system for the computation of both the corresponding observables. In Table 5 we show the condition numbers $\text{cond}_{\text{model}}$ of the matrices of coefficients of linear systems (17) obtained in the case of lung data with $\mu_m = 10^{-3}$ and "model" assuming the values gomp, exp, gen log, von bert and power in correspondence of the Gompertz, exponential, generalized logistic, von Bertalanffy–West and power-law growth laws, respectively. As one can see, in most of the cases such condition numbers are very close to 1 and in general are not greater than 2. Similar results are obtained for breast data and different choices of the parameter μ_m.

All the computations have been performed in double precision arithmetics.

Table 5
Condition numbers $\text{cond}_{\text{model}}$ of the coefficient matrices of linear systems (17) obtained in the case of lung data with $\mu_m = 10^{-3}$ and "model" assuming the values gomp, exp, gen log, von bert and power in correspondence of the Gompertz, exponential, generalized logistic, von Bertalanffy–West and power-law growth laws, respectively.

n	j	$\text{cond}_{\text{gomp}}$	cond_{exp}	$\text{cond}_{\text{gen log}}$	$\text{cond}_{\text{von bert}}$	$\text{cond}_{\text{power}}$
8	5	1.000749	1.00000044	1.022885	1.001474	1.748742
16	10	1.000803	1.00000056	1.038327	1.001777	1.802614
32	19	1.000829	1.00000062	1.038343	1.001768	1.842141
64	39	1.000823	1.00000068	1.038273	1.001762	1.751541
128	78	1.000817	1.00000074	1.038273	1.001761	1.749672
256	156	1.000836	1.00000080	1.038293	1.001774	1.749009
512	312	1.000837	1.00000084	1.043274	1.001892	1.838238

5.1. Data and parameter values

The parameter values for the growth laws introduced (Table 1) were computed in [3]. Benzekry et al. used data from two different in vivo systems. The first is a syngeneic Lewis lung carcinoma (LLC) mouse model and the second one is an orthotopic human breast cancer xenografted in severe combined immunodeficient (SCID) mice, that for the sake of simplicity we will indicate with lung and breast tumors, respectively. In Table 2 the parameter values for lung (third column) and breast (fourth column) data are reported. We also fix the initial values of the primary tumor $v_{p,0} = 1$ mm^3, that corresponds to the size of the tumor implanted in the mice, and of the secondary tumor, $v_{m,0} = 10^{-6}$ mm^3. Moreover in the metastasis emission rate $\beta(t)$ we first assume $\mu_p = \mu_m = 10^{-3}$ day^{-1} mm$^{-3\alpha}$ and $\alpha = 2/3$, [2]. Notice that whenever different values than those introduced above will be used, the new values will be specified in the text accordingly.

5.2. Simulation results

The biological observables defined in (3) for the PDE model (1) are computed assuming that the primary and secondary tumors growth functions are the same. Moreover, these functions can assume one of the five expressions introduced in Table 1. First let us focus our attention on the five different curves within the same case study, and secondly comparing the different tumors. Notice that, in the figures below, we used a semilog plot for the y axis.

In Fig. 1 the metastatic mass $M(t)$ (left panel) and the cumulative number of metastases $N_{\bar{v}(t)}$ (right panel) for the lung tumor data are plotted. Here we have focused our attention on these two different observables because they are the main quantities available from tumor imaging detection. Analyzing the results for the metastatic mass (left panel in Fig. 1) one can see that the higher value corresponds to the generalized logistic growth law followed by power-law, while the total masses are the smallest one for von Bertalanffy–West, exponential and Gompertz growth laws. Moreover, looking at the right panel in Fig. 1, one can see that for an interval of time close to 20 days the Gompertz, power-law and exponential growth laws have as outcome a cumulative number of metastases greater than $\bar{v} = 10^{-6}$ mm^3 that is more or less equal. Whereas, at the end of 60 days the von Bertalanffy–West growth law is the one with the smallest number of metastases and the remaining four have comparable values.

In Fig. 2 the results for breast tumor data are plotted. Here differently than for lung data, von Bertalanffy–West is the growth law that generates the highest total metastatic mass, followed by power law, generalized logistic and Gompertz laws, and last exponential law. In the right panel, instead, one can see that von Bertalanffy–West growth law is the only one that generates the highest cumulative number of metastases greater than $\bar{v} = 10^{-6}$ mm^3 while interestingly the remaining ones behave in a similar way.

Comparing the outcomes of the two case studies, it is clear that Gompertz and exponential laws are the ones that generate the lowest metastatic mass for both cases, while for the remaining four laws the results depend on the considered case. Surprisingly von Bertalanffy–West law generates the highest cumulative number for breast data and on the opposite the lower value for the lung case. Another similarity between the two cases is that the curves corresponding to the number of metastases for the remaining growth laws are comparable in between them for a short (lung) or long (breast) interval of time.

In Fig. 3 we have analyzed how the total metastatic mass changes assuming that the colonization coefficient, μ_*, is different for the primary (μ_p) and secondary (μ_m) tumor. Moreover, we assumed that the colonization coefficient

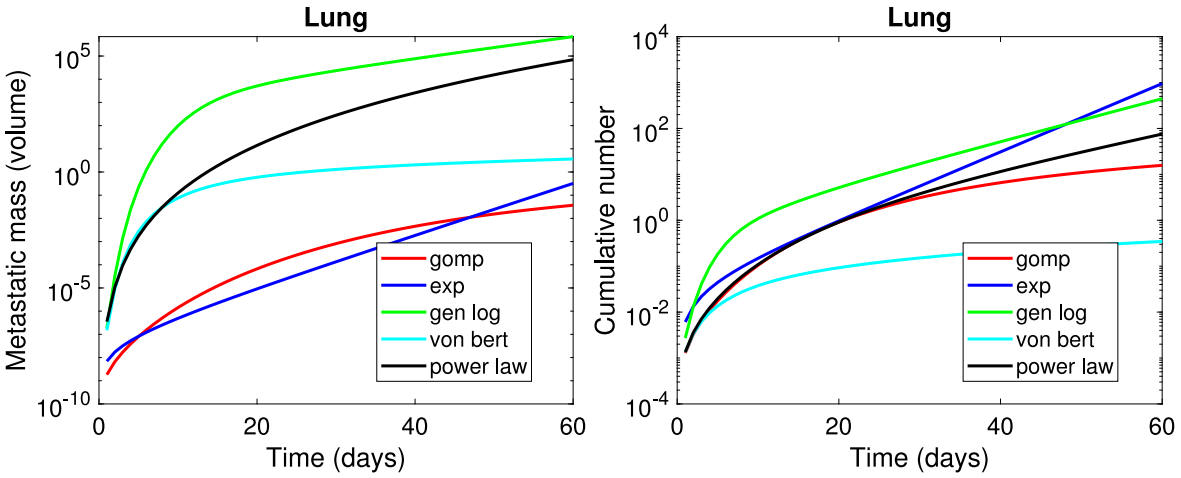

Fig. 1. The metastatic mass (left panel) and the cumulative number of metastases (right panel) for the lung tumor case. Notice that we used a semilog plot for the y axis.

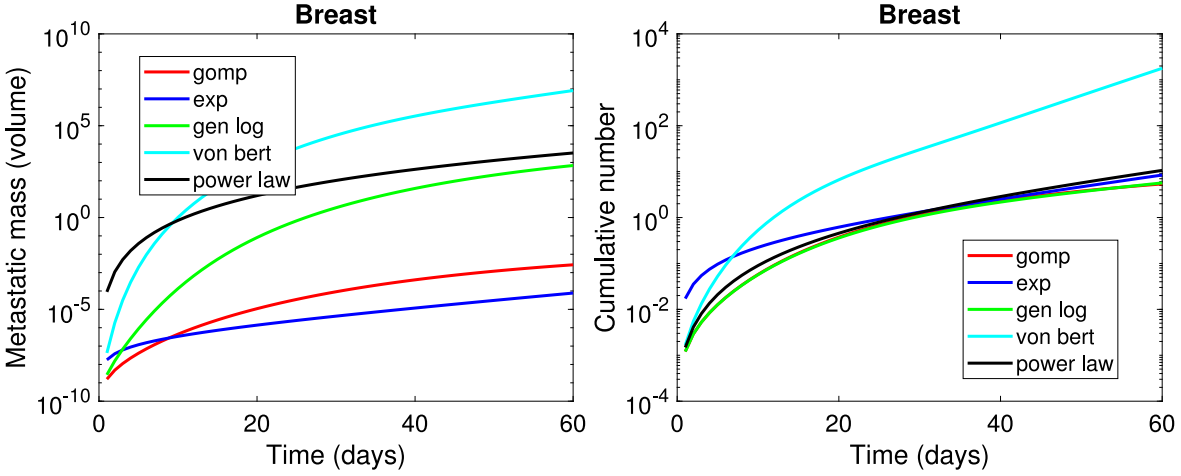

Fig. 2. The metastatic mass (left panel) and the cumulative number of metastases (right panel) for the breast tumor case. Notice that we used a semilog plot for the y axis.

corresponding to the metastases can be either $\mu_m = 0$ or $\mu_m = 10^{-3}$. In the first case it means that the metastases are emitted only by the primary tumor. Once fixed the value of μ_m we vary μ_p taking three different values $\mu_p = 10^{-4}$, $\mu_p = 10^{-3}$ or $\mu_p = 10^{-2}$, [2]. For both lung and breast tumor case studies, increasing μ_p leads to a growth of the metastatic mass volume (see the differences between dashed, continuous and dotted lines). More importantly, if we consider the lung tumor (first row of Fig. 3) one can see that the metastatic mass for exponential, von Bertalanffy–West and Gompertz growth laws maintain close values for $\mu_m = 0$ or $\mu_m = 10^{-3}$, while for both generalized logistic and power-law growths, increasing μ_m leads to a growth in the metastatic mass. For the breast tumor case instead there is no significant growth in the tumor mass assuming that the metastases emit metastases themselves.

As our last result, we have investigated how the total metastatic mass changes assuming that the initial size of the new metastasis $v_{m,0}$ is greater than 1 cell (10^{-6} mm^3). In Figs. 4–5 we have represented five different surfaces (top row) corresponding to the five different growth laws, for each case study (Fig. 4 for lung and Fig. 5 for breast). Each surface is obtained by fixing all the parameter values as in Table 2, with exception of $v_{m,0}$ that assumes ten equispaced values in the interval $\left[10^{-6}, 10^{-5}\right]$. On the bottom row of Figs. 4–5 we have represented the $x - z$ projection of the surfaces plotted on the bottom row, that corresponds to a time-metastatic mass projection. From this last plot it is evident that not for all five tumor growth laws increasing $v_{m,0}$ will lead to a higher/lower total

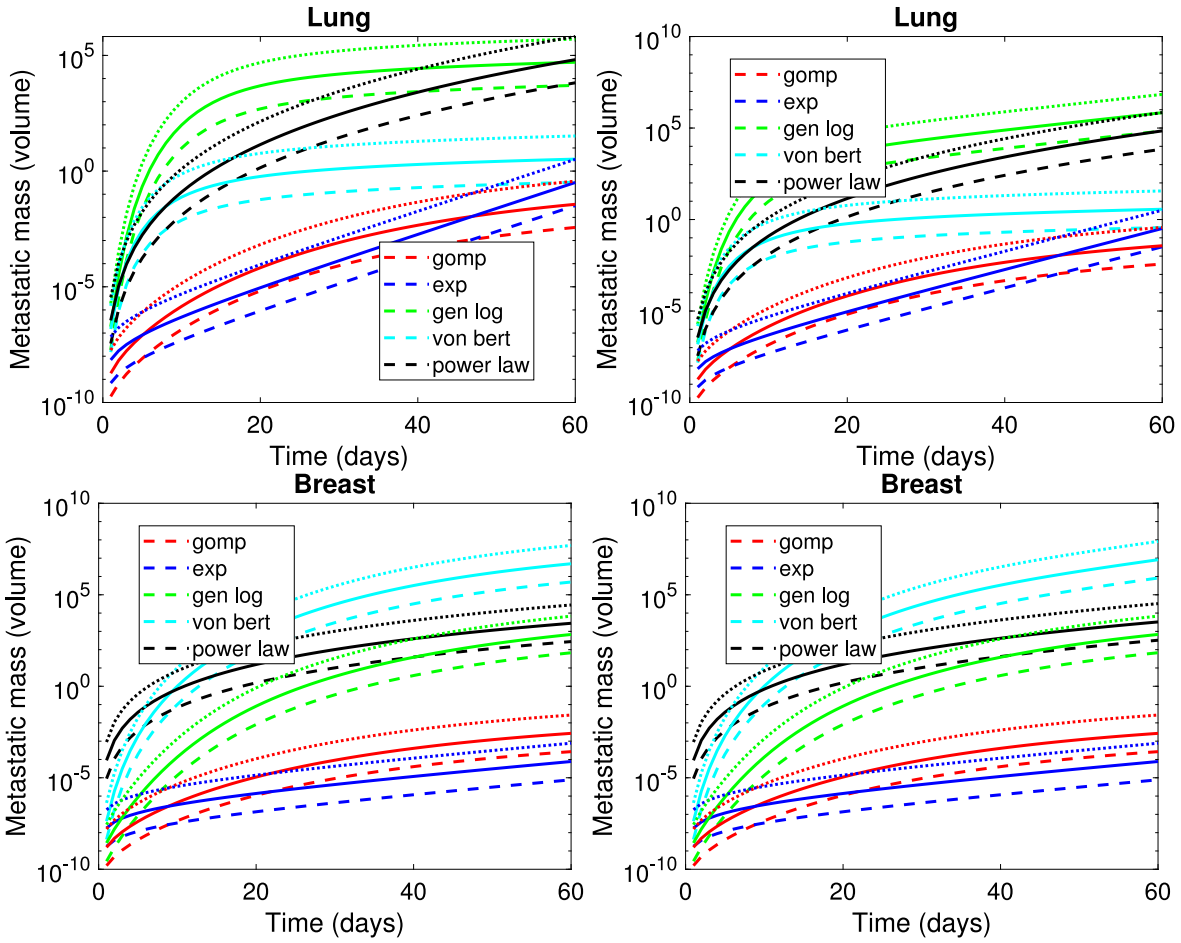

Fig. 3. Left panel: The metastatic mass for $\mu_m = 0$; Right panel: The metastatic mass for $\mu_m = 10^{-3}$. Top row: lung, bottom row: breast. Dashed lines $\mu_p = 10^{-4}$, continuous line $\mu_p = 10^{-3}$, dotted line $\mu_p = 10^{-2}$. Notice that we used a semilog plot for the y axis.

metastatic mass, in fact for the thickest lines (exponential and Gompertz growth laws) this happen while for the thinnest lines not (generalized logistic, von Bertalanffy–West and power-law).

6. Discussion and conclusions

In this paper we propose an alternative and efficient numerical method for the resolution of Partial Differential Equation (PDE) models, describing the metastatic tumor growth, reformulated in terms of VIEs of second kind in the same fashion of [18]. It is a modified version of the method proposed in [11] for the numerical computation of long-time solutions of linear Volterra integral equations of the second kind. The introduced modifications are crucial in order to increase the accuracy in the approximation of the observables. Moreover, further general properties of this method are: its flexibility in solving a wide range of VIE, not necessarily of convolution type (as required by FFT based methods), also derived from applications; whatever is the number of the evaluation times only one linear system has to be solved; its convergence in weighted spaces of continuous functions as shown by the provided error estimates in weighted uniform norm. A weaknesses of the proposed method might be related to the computational complexity in the construction of the entries of the matrix and the right-hand sides of the linear system. Further investigation in order to reduce such complexity will be carried out in a future work.

In this paper we have considered a generalized version of the mathematical model proposed by Iwata and coauthors in [20], which describes metastatic tumor growth. The novelties introduced are three: (i) We have assumed five different tumor growth laws for both primary and secondary tumor growths (exponential, power-law, Gompertz,

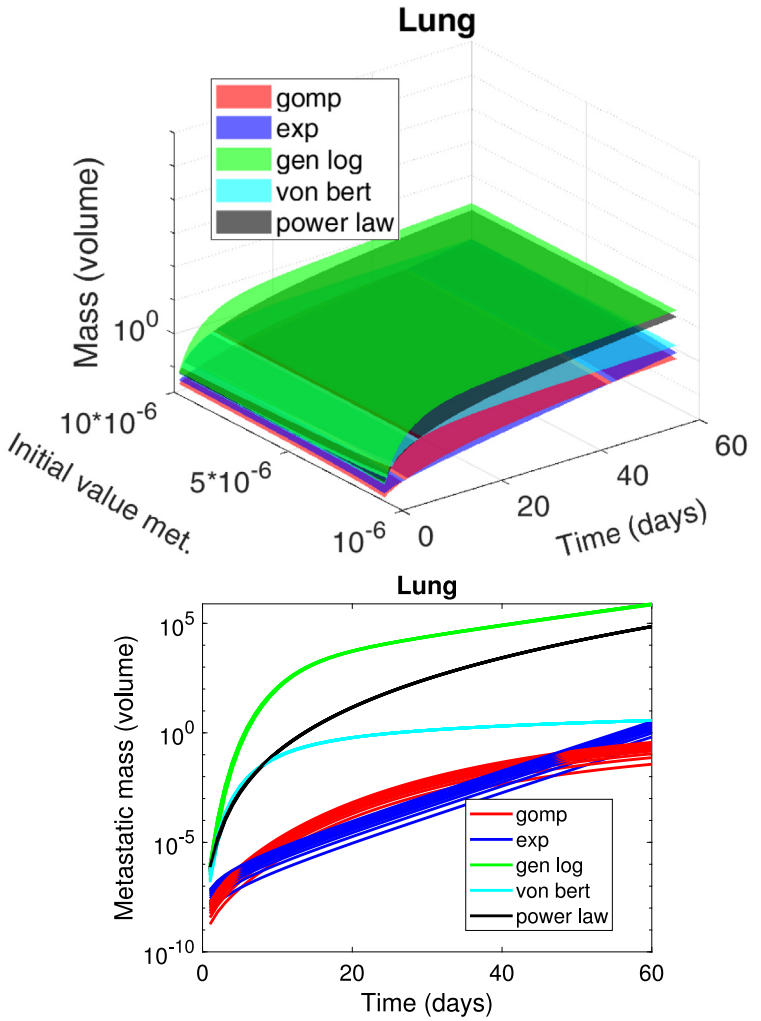

Fig. 4. Top row: the metastatic mass for each tumor growth function for an interval of time of 60 days and 10 different values of $v_{m,0}$ that assumes equispaced values in the interval $[10^{-6}, 10^{-5}]$ fixing the other parameter values as in Table 2. Bottom row: the $x - z$ projection of the top plot.

generalized logistic and von Bertalanffy–West). (ii) We have considered different metastatic emission rates for the primary and metastases themselves. (iii) Last, we have assumed that the newborn metastases can be formed by clusters of several cells.

We did the numerical simulations for two different case studies, lung and breast tumors. Comparing the five different curves within the same type of tumor, we can conclude that (i) for lung tumor case (see Fig. 1) Gompertz and exponential growth laws behave in a similar way, the same for generalized logistic and power-law growths, while the von Bertalanffy–West is in between the two cases. This can be seen for metastatic mass while for the cumulative number of metastases von Bertalanffy–West growth law is the one that behaves dissimilar from the remaining four growth laws. (ii) Differently, for the growth of the metastatic mass of a breast tumor (see Fig. 2) von Bertalanffy–West growth law has the most dissimilar behavior, while, at the end of the 60 days, power-law and generalized logistic reach comparable values as well as the exponential and Gompertz laws. For the cumulative number of metastases, instead, only von Bertalanffy–West growth law behaves differently than the remaining four ones.

Assuming that the emission rate of the metastases is different for primary and secondary tumor, respectively, we can conclude that fixing the colonization coefficient for the secondary tumors and increasing the coefficient

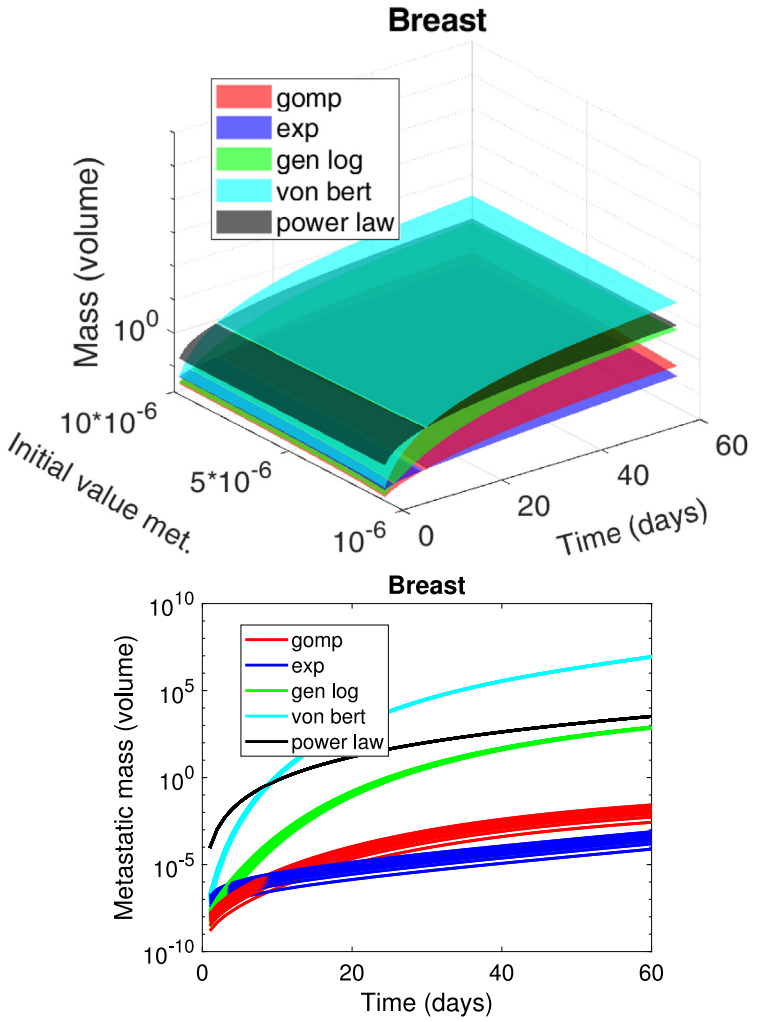

Fig. 5. Top row: the metastatic mass for each tumor growth function for an interval of time of 60 days and 10 different values of $v_{m,0}$ that assumes equispaced values in the interval $\left[10^{-6}, 10^{-5}\right]$ fixing the other parameter values as in Table 2. Bottom row: the $x-z$ projection of the top plot.

of the primary tumor leads to a growth of the total metastatic mass. Interestingly, assuming that the metastases will not generate metastases themselves will affect, more significantly, the metastatic mass only for power-law and generalized logistic laws, for lung data, while no relevant changes occur for breast data. Given the biological evidence, [9], that the "newborn" metastases can be formed by clusters of cells, from our numerical results obtained, assuming that the clusters sizes can vary from 1 to 10 cells, we can conclude that the metastatic mass increases with increasing the initial value of the metastasis size in a more accentuated way for Gompertz and exponential growth laws, but not for the remaining three growth laws.

We are aware that the chosen growth law models and consequently the parameter values might not reproduce reality but we are optimistic that the flexibility of the introduced method, that solves the PDE–ODE model, will permit the study of different types of tumors and growth functions. As further developments we would like to extend the method also (i) for growth laws for which the analytical solution is not known, and (ii) for the 2D ODE system case which includes the cure of the tumor.

Declaration of competing interest

The authors declare that they have no known competing financial interests or personal relationships that could have appeared to influence the work reported in this paper.

Acknowledgments

IMB has been supported by MUR through the grant PON-AIM Linea 1 (AIM1852570-1). MCDB and CL have been supported by University of Basilicata, Italy (local funds). IMB, MCDB and CL have been supported by GNCS Project 2020 “Approssimazione multivariata ed equazioni funzionali per la modellistica numerica”. This research has been accomplished within RITA (Research ITalian network on Approximation) and the UMI Group TAA (Approximation Theory and Applications).

References

[1] C.H.T. Baker, A perspective on the numerical treatment of Volterra equations, J. Comput. Appl. Math. 125 (2000) 217–249.
[2] S. Benzekry, Mathematical and numerical analysis of a model for anti-angiogenic therapy in metastatic cancers, ESAIM Math. Model. Numer. Anal. - Modél. Math. Anal. Numér. 46 (2) (2012) 207–237.
[3] S. Benzekry, C. Lamont, A. Beheshti, A. Tracz, J.M.L. Ebos, L. Hlatky, P. Hahnfeldt, Classical mathematical models for description and prediction of experimental tumor growth, PLoS Comput. Biol. 10 (2014) 1–19.
[4] C. Berkel, E. Cacan, Metastases from metastases: comparative metastatic potential of human cancer cell lines originated from primary tumors or metastases in various tissues, J. Cell Commun. Signal. 15 (2021) 461–464.
[5] A. Bethge, U. Schumacher, A. Wree, G. Wedemann, Are metastases from metastases clinical relevant? Computer modelling of cancer spread in a case of hepatocellular carcinoma, PLoS One 7 (4) (2012) 1–12.
[6] H. Brunner, A survey of recent advances in the numerical treatment of Volterra integral and integro-differential equations, J. Comput. Appl. Math. 8 (1982) 213–229.
[7] H. Brunner, Collocation Methods for Volterra Integral and Related Functional Equations, in: Cambridge Monographs on Applied and Computational Mathematics, vol. 552, Cambridge University Press, Cambridge, 2004.
[8] C.L. Chaffer, R.A. Weinberg, A perspective on cancer cell metastasis, Science 331 (2011) 1559–1564.
[9] K.J. Cheung, V. Padmanaban, V. Silvestri, K. Schipper, J.D. Cohen, A.N. Fairchild, M.A. Gorin, J.E. Verdone, K.J. Pienta, J.S. Bader, A.J. Ewald, Polyclonal breast cancer metastases arise from collective dissemination of keratin 14-expressing tumor cell clusters, Proc. Natl. Acad. Sci. USA 113 (E) (2016) 854–863.
[10] M.C. De Bonis, B. Della Vecchia, G. Mastroianni, Approximation of the Hilbert transform on the real semiaxis using Laguerre zeros, J. Comput. Appl. Math. 140 (2002) 209–229.
[11] M.C. De Bonis, C. Laurita, V. Sagaria, A numerical method for linear Volterra integral equations on infinite intervals, Appl. Numer. Math. 172 (2022) 475–496.
[12] M.C. De Bonis, D. Occorsio, On the simultaneous approximation of a Hilbert transform and its derivatives on the real semiaxis, Appl. Numer. Math. 114 (2017) 132–153.
[13] Z. Ditzian, On interpolation of $L^p[a,b]$ and weighted Sobolev spaces, Pacific J. Math. 90 (2) (1980) 307–323.
[14] I.J. Fidler, The pathogenesis of cancer metastasis: the ‘seed and soil’ hypothesis revisited, Nat. Rev. Cancer 3 (6) (2003) 453–458.
[15] L.C. Franssen, T. Lorenzi, A.E.F. Burgess, M.A.J. Chaplain, A mathematical framework for modelling the metastatic spread of cancer, Bull. Math. Biol. 81 (6) (2019) 1965–2010.
[16] P. Friedl, K. Wolf, Tumour-cell invasion and migration: diversity and escape mechanisms, Nat. Rev. Cancer 3 (5) (2003) 362–374.
[17] E. Hairer, C. Lubich, M. Schlichte, Fast numerical solution of nonlinear Volterra convolution equations, J. Sci. Statist. Comput. 5 (1985) 532–541.
[18] N. Hartung, Efficient resolution of metastatic tumor growth models by reformulation into integral equations, Discrete Contin. Dyn. Syst. Ser. B 20 (2) (2015) 445–467.
[19] N. Hartung, S. Mollard, D. Barbolosi, A. Benabdallah, G. Chapuisat, G. Henry, S. Giacometti, A. Illiadis, J. Ciccolini, C. Faivre, H. Hubert, Mathematical modeling of tumor growth and metastatic spreading: Validation in tumor-bearing mice, Cancer Res. 74 (2014) 6397–6407.
[20] K. Iwata, K. Kawasaki, N. Shigesada, A dynamical model for the growth and size distribution of multiple metastatic tumors, J. Theoret. Biol. 203 (2000) 177–186.
[21] P. Junghanns, G. Mastroianni, I. Notarangelo, On Nyström and product integration methods of Fredholm integral equations, in: Contemporary Computational Mathematics - a Celebration of the 80th Birthday of Ian Sloan, 2018, pp. 645–673.
[22] A.W. Lambert, D.R. Pattabiraman, R.A. Weinberg, Emerging biological principles of metastasis, Cell 168 (2017) 670–691.
[23] C. Laurita, G. Mastroianni, L^p-Convergence of Lagrange interpolation on the semiaxis, Acta Math. Hungar. 120 (4) (2008) 249–273.
[24] G. Mastroianni, G.V. Milovanović, Some numerical methods for second-kind Fredholm integral equations on the real semiaxis, IMA J. Numer. Anal. 29 (2009) 1046–1066.
[25] G. Mastroianni, G. Monegato, Truncated Gauss-Laguerre quadrature rules, in: D. Trigiante (Ed.), Recent Trends in Numerial Analysis, Vol. 3, Nova Sci. Publ., Huntington, NY, 2001, pp. 213–221.
[26] G. Mastroianni, D. Occorsio, Numerical approximation of weakly singular integrals on the half-line, J. Comput. Appl. Math. 140 (1–2) (2002) 587–598.

[27] F. Mirzaee, E. Hadadiyan, A new numerical method for solving two-dimensional Volterra-Fredholm integral equations, J. Appl. Math. Comput. 52 (2016) 489–513.
[28] F. Mirzaee, S.F. Hoseini, Application of Fibonacci collocation method for solving Volterra-Fredholm integral equations, Appl. Math. Comput. 273 (2016) 637–644.
[29] F. Mirzaee, S.F. Hoseini, A new collocation approach for solving systems of high-order linear Volterra integro-differential equations with variable coefficients, Appl. Math. Comput. 311 (2017) 272–282.
[30] J.S. Spratt, J.S. Meyer, J.A. Spratt, Rates of growth of human solid neoplasms: Part I, J. Surg. Oncol. 60 (1995) 137–146.
[31] J.E. Talmadge, I.J. Fidler, AACR centennial series: The biology of cancer metastasis: Historical perspective, Cancer Res. 70 (14) (2010) 5649–5669.
[32] J.E. Talmadge, S.R. Wolman, I.J. Fidler, Evidence for the clonal origin of spontaneous metastasis, Science 217 (1982) 361–363.
[33] J.E. Talmadge, B. Zbar, Clonality of pulmonary metastases from the bladder 6 subline of the B16 melanoma studied by southern hybridization, J. Natl. Cancer Inst. 78 (1986) 315–320.